CONF-950793--9

NREL/TP-452-8106 • UC Category: 1600 • DE95009262

Spectral Selectivity of Electrochromic Windows with Color State for All-Sky Conditions

RECEIVED
AUG 0 4 1995
OSTI

D. E. Soule, J-G. Zhang, D. K. Benson

Prepared for the SPIE Optical Materials Technology for Energy Efficiency and Solar Energy Conversion XIV
July 9–14, 1995
San Diego, California

National Renewable Energy Laboratory
1617 Cole Boulevard
Golden, Colorado 80401-3393
A national laboratory of the U.S. Department of Energy
Managed by Midwest Research Institute
for the U.S. Department of Energy
under contract No. DE-AC36-83CH10093

Prepared under Task No. ER480101

July 1995

NOTICE

This report was prepared as an account of work sponsored by an agency of the United States government. Neither the United States government nor any agency thereof, nor any of their employees, makes any warranty, express or implied, or assumes any legal liability or responsibility for the accuracy, completeness, or usefulness of any information, apparatus, product, or process disclosed, or represents that its use would not infringe privately owned rights. Reference herein to any specific commercial product, process, or service by trade name, trademark, manufacturer, or otherwise does not necessarily constitute or imply its endorsement, recommendation, or favoring by the United States government or any agency thereof. The views and opinions of authors expressed herein do not necessarily state or reflect those of the United States government or any agency thereof.

Available to DOE and DOE contractors from:
Office of Scientific and Technical Information (OSTI)
P.O. Box 62
Oak Ridge, TN 37831
Prices available by calling (615) 576-8401

Available to the public from:
National Technical Information Service (NTIS)
U.S. Department of Commerce
5285 Port Royal Road
Springfield, VA 22161
(703) 487-4650

Printed on paper containing at least 50% wastepaper and 10% postconsumer waste

DISCLAIMER

Portions of this document may be illegible in electronic image products. Images are produced from the best available original document.

Spectral selectivity of electrochromic windows with color state for all-sky conditions*

David E. Soule+

Western Illinois University, Department of Physics
Macomb, Illinois 61455

Ji-Guang Zhang and David K. Benson

National Renewable Energy Laboratory
1617 Cole Blvd., Golden, Colorado 80401

ABSTRACT

The optical performance of an electrochromic window is studied for the visible, ultraviolet, and near infrared spectral regions. The performance is found to deviate strongly with window color state and for clear or cloudy skies. A new spectral cloud model (Soule et al) is applied to an electrochromic window recently developed at NREL (Zhang and Benson). A spectral comparison is made between the electrochromic window and spectrally selective standard windows. Two series of double-glazed window sections, including the electrochromic window with color state and a series of low-E windows, were measured for transmittance and reflectance (300 - 2500nm). With these spectral data, a new near-infrared blocking (reflection + absorption) factor is developed for window application in warm climates for cooling load reduction. A chromaticity analysis is presented for both the daylight spectra and the transmitted electrochromic window spectra with color state. Computed daylight correlated color temperatures show a wide range, with values of 5660K for clear global irradiation, 6210K for clouds, and 13,250K for a zenith blue sky. Chromatic trajectories with color state for transmitted radiation extend further toward the blue to 8180K for the global and 28,990K for zenith sky irradiation.

1. INTRODUCTION

The solar irradiance transmitted through electrochromic (EC) windows changes with color state of the window and is a strong function of the detailed spectral profile of both the window and of the sky. Many of the important functional performance characteristics of the EC window are significantly altered in cloudy climates. Daylighting color shift, solar heat gain, degradative UV transmission, and cooling load reduction potential are all sensitive to changes in the sky conditions. Along with a reduced visible transmittance, there is typically a blue shift caused by the darkened electrochromic coating. This color shift is further modified by the cloudy-sky solar spectrum.

In this paper, we use a newly developed computer model for cloudy skies of Soule et al,[1] along with optical transmittance and reflectance measurements to predict the optical performance of a typical experimental EC window developed at NREL by Zhang et al.[2] The cloud model includes the cloud/atmosphere/ground optical components - cloud top albedo, cloud absorption, UV cloud enhancement, and cloud/ground multi-reflection. The EC window performance is studied for the cloudy-sky solar spectrum and

*Supported by U. S. Department of Energy, Contract DE-AC36-83-CH10093
+On leave from Western Illinois University, Macomb, IL 61455

MASTER

DISTRIBUTION OF THIS DOCUMENT IS UNLIMITED

for two standard clear-sky solar spectra (global and blue sky) under identical assumptions of atmospheric parameters.

Optical measurements were made of the spectral transmittance and reflectance (300 - 2500nm) on two double-glazed window series:

A. NREL electrochromic (EC) window for five color states, from the bleached state (1) to a highly colored state (5).

B. Spectrally selective (SS) windows with spectral selectivity, from the conventional sodalime silicate double-glazed window, to low-E windows; one with a tin oxide coating and a second with a tin-doped indium oxide (ITO) coating.

New window performance factors were developed for evaluating the extent of blocked solar flux (reflected + absorbed), as applied to both the near infrared (NIR) and the ultraviolet (UV). These sky sensitive blocking factors have the potential for predicting window performance in warm climates for NIR cooling load reduction and for reducing UV material degradation.

A chromaticity analysis was performed on both the incident daylight spectra and on the EC window transmitted spectra. Wide ranges in chromaticity were found in both the daylight, from the cloudy sky to the blue zenith sky, and in the EC transmitted spectra, from the bleached to the highly colored state. Resultant correlated color temperatures also show corresponding large shifts in color for this electrochromic window under realistic sky conditions.

2. WINDOW SERIES

A double-glazed window configuration was chosen for this optical study to represent a typical operational window crossection. Sample window sections (3.8 cm x 7 cm) for optical measurements are shown in Fig. 1, where sodalime silicate (SLS) (3mm) glass is used for the second pane, with the exception of the EC window where a borosilicate (BRS) (3mm) glass is used to minimize window color distortion.

These window sections are arranged from the standard double-glazed sodalime silicate window (SLSD), progressing to the Low E windows: tin oxide coated (SNOD) and tin-doped indium oxide (ITOD), and then to the electrochromic (EC) window (Z4D). They are oriented to show the direction of the incident solar flux (S) and also show the location of the Low E and EC films on side #2 for optimal summer operation.

2.1. Electrochromic window series

The electrochromic window investigated here was developed at NREL by Zhang et al.[2] It consists of a multilayer (WO_3 + Li-polymer electrolyte + V_2O_5) sandwiched between ITO-coated sodalime silicate glass (SLS) panes. In the double-glazed window configuration (Z4D) of this optical study, the overall crossection is given by,

$$[\mathrm{SLS(2mm)} + \mathrm{ITO} + \mathrm{WO_3} + \mathrm{Li\text{-}poly.elec.} + \mathrm{V_2O_5} + \mathrm{ITO} + \mathrm{SLS(2mm)}]$$

$$/\ \mathrm{Air\ (1mm)}\ /\ \mathrm{BRS\ (3mm)}\ .$$

A range of five color states extending from the bleached state (1) to the highly colored state (5) is chosen here. These states, designated here as separate windows

in the EC series, are described in Table 1. The applied potential (P) was chosen as the experimental parameter representing the color state. Alternatively, the potential difference (PD), defined by PD = 1.2 - P, was found to be convenient for analysis in this study, as referenced to the bleached state potential.

2.2 Spectrally selective window series

The double-glazed windows in the SS window series are scaled in spectral selectivity from the double-glazed SLS typical window (SLSD) to the highly selective Low-E windows SNOD and ITOD. These windows are described in Table 2, where a single-glazed DSA (3mm) SLS window is also added to provide a standard for comparison.

2.3 Window section optical measurements

Near-normal spectral transmittance $T(\lambda)$ and reflectance $R(\lambda)$ measurements were made on a Perkin-Elmer Lambda-9 spectrophotometer from 300nm to 2500nm at 10nm wavelength (λ) intervals. Spectral absorptance $A(\lambda)$ was further computed from $A(\lambda) = 1 - T(\lambda) - R(\lambda)$. In Fig. 2A are shown the electrochromic window spectral transmittance curves for the five color states extending from the bleached state (1) to the highly colored state (5). It is noted that these curves progressively change both in magnitude and in contour, as will be analyzed chromatically below. The spectral reflectance curves in Fig. 2B seem to be relatively constant in contour throughout the color state range. This behavior appears to be dominated by the ITO base coatings in the EC multilayer described above, since this reflectance contour is similar to the ITOD reflectance contour (not shown). On the other hand, the spectral absorptance curves in Fig. 2C vary significantly showing that the darkening in the EC window with color state is due primarily to the absorptance change.

2.4 Visible and solar transmittance

A wide potential range for window applications computed for daylighting/visibility and effective solar gain are shown by the sky-averaged visible transmittance (T_V) and solar transmittance (T_S) in Fig. 3. Both the EC and SS window series are displayed for overall comparison. As shown in the figure, T_V ranges from 89.6% for the reference window SLS to 70.1% for the highly selective ITOD window and from 62.7% (or 68.9% for a single EC pane) for the bleached state Z4D1 to 25.9% for the highly colored state Z4D5- an overall drop of 63.7% in visibility. Correspondingly, T_S extends from 83.3% to 56.0% for the SS series and from 53.4% to 16.4% for the EC series, respectively - an overall drop of 66.9% in solar transmittance.

For the electrochromic window Z4D, the relative attenuation in T_V from the bleached state (1) to the highly colored state (5) is 59%, as a measure of shading efficiency. With solar transmittance, the corresponding relative drop in T_S is 69%, demonstrating the significant potential of this window for solar applications as well.

3. ALL-SKY SPECTRA

One objective in this study was to generate representative incident solar spectra (300 - 2500nm) in the ALLSKY1 model for a range of sky conditions encountered in typical window applications. Three model spectra were developed: the cloudy-sky irradiance (C), the clear-sky global horizontal irradiance (G), and the clear blue-sky irradiance (S).

The cloud-modified solar spectrum (C) was derived from the CLDSPEC3 cloud model of Soule et al.[1] This three-atmosphere layer model, as incorporated into 2-stream theory, includes the cloud/atmosphere/ground optical components: cloud top albedo, cloud absorption, ultraviolet (UV) cloud enhancement, and cloud/base/ground cover multireflection. For this case, the UV enhancement factor was fitted to the measured overcast spectrum[3] for Cape Canaveral, FL for 9/30/87 at 12:31 EST with AM 1.2. The resultant model cloud spectrum, as normalized to the observed spectrum and adjusted for the UV enhancement factor, fitted to within ± 2.9% for wavelengths from 320 to 670nm.

For the clear-sky layers within the overall three-layer cloud model, the Bird and Riordan[4] clear-sky model SPCTRAL2 was used to specify the instantaneous solar spectra. In addition, the clear-sky global spectra (G) and sky spectra (S) were developed from SPCTRAL2.

To make a proper spectral comparison between these three solar spectra, C, G, and S; a near standard solar zenith angle (Airmass = 1.2) was used throughout and the atmospheric parameters were matched. The specific parameters used were those used for modelling the clear-sky layers of the measured overcast cloud case mentioned above, including water vapor (4.80 cm), turbidity (0.25), Angstrom alpha (0.93) and ozone (0.15 ATM cm).[3] The three resultant atmospherically matched spectra for the above date, time, and location would have broadband totals of, 247 w/m^2 for C, 860 w/m^2 for G, and 186 w/m^2 for S.

The G, C, and S solar spectra are normalized in Fig. 3, facilitating a direct comparison of their respective spectral contours for given wavelength ranges. These spectral contours are seen to be significantly different in the UV (310nm - 400nm) and near infrared (NIR) (700nm - 2500nm) wavelength ranges, as demonstrated by the irradiance spectral fractions in Table 3. It is significant that while the fractional irradiance rank ordering for UV is S, C, G; the reverse is true for NIR - G, C, S.

4. SPECTRAL SELECTIVITY

The relative spectral selectivities of the double-glazed windows included in this study are shown by the spectral transmittance contours given in Fig. 2A for the EC window series with color state and in Fig. 2D for the SS window series with spectral selectivity. One convenient indicator of spectral selectivity from these data, where the transmittance is maximized in the visible (560nm) and minimized in the infrared (2500nm), is given by, T-ratio = T(560nm)/T(2500nm). Ratios are compared in order of selectivity for the SLSD, SNOD, Z4D1 (bleached), and ITOD windows in Table 4.

The degree of spectral selectivity is important primarily in maximizing the visible transmittance (T_V), while simultaneously minimizing the infrared transmittance. Two objectives of cold or warm climate window performance, however, involve different relevant infrared regions - the incident solar spectrum or the emissive blackbody spectrum, which do not overlap. These two infrared regions are related to the energy flow equation, Eq. 1 from Soule,[5] where it was shown that the solar flux (optical) or blackbody emission (thermal) dominate according to winter or summer use. These infrared regions are involved for cold or warm climate use by,

A. Minimizing $T(\lambda)$ centered near 10μm, where the blackbody emittance peak occurs

for the ASHRAE average temperature of 288K.[6,7] The Low-E window concept stresses this approach[8] for lowering the window thermal loss in winter.

B. Minimizing $T(\lambda)$ in the near infrared (NIR) solar region (700 - 2500nm) to block (reflection + absorption) excessive input solar heat. This approach applies to cooling load reduction for summer and/or warm climate applications.

A blocking factor for the NIR solar region is introduced here that gives the fraction of the incident solar flux that is blocked (reflected + absorbed). This factor $BT_{IR}(i,j)$, that depends on the specific incident solar spectrum (i) (G, C, or S) and on the window type (or color state) (j), is given by,

$$BT_{IR}(i,j) = \frac{\int_{700nm}^{2500nm} [1 - T(j)]E(i)d\lambda}{E_T(i)} , \qquad (1)$$

where $E_T(i)$ = equivalent broadband incident solar flux. This integrated flux E_T is typically measured at widely distributed sites, thus making this approach convenient for window performance predictions.

A similar methodology is applied here to the UV range 310 - 400nm (approximately UV-A), where in this case internal UV material degradation is to be avoided. The corresponding UV blocking factor is given by,

$$BT_{UV}(i,j) = \frac{\int_{310nm}^{400nm} [1 - T(j)]E(i)d\lambda}{E_T(i)} . \qquad (2)$$

These blocking factors are found to be significantly affected by both the window type (or color state) and by the sky condition (G, C, S), as shown in Fig. 5, including the combined SS and EC series. For the UV and NIR ranges with global sky, these deviations with window type are,

$$BT_{UV} = 1.7\% \rightarrow 4.4\% \rightarrow 5.9\%$$

$$BT_{IR} = \underset{(SLS)}{10\%} \rightarrow \underset{(Z4D1)}{27.0\%} \rightarrow \underset{(Z4D5)}{44.6\%} .$$

In the UV, these deviations differ by an overall factor of 3.5 from the standard SLS window to the highly colored Z4D5 window. For the NIR range, the deviation is by a factor of 4.5 for the same window range.

Also as seen in Fig. 5, these factors show a wide divergence with sky condition from the standard clear-sky global sky (G) to the cloudy sky (C) and then to the blue sky (S). For the EC color state (5) window Z4D5, these divergences are,

$$BT_{UV} = 5.9\% \rightarrow 9.4\% \rightarrow 12.4\%$$

$$BT_{IR} = \underset{(G)}{44.6\%} \rightarrow \underset{(C)}{35.4\%} \rightarrow \underset{(S)}{26.9\%} .$$

These deviations also show reverse trends for the UV and NIR ranges, increasing by a factor of 2.1 for the UV and decreasing by a factor of 1.7 for the NIR from the standard G spectrum.

5. DAYLIGHT AND EC WINDOW CHROMATICITY

In the visible range, both the daylight solar spectra with sky conditions and the electrochromatic window with color state show spectral shifts in color. These color shifts are shown for four distinct sky spectra in Fig. 6A and for the transmittance at five color states of the EC window in B. The luminous response curve L is also included for a chromatic perspective.

In the daylight spectral series, a new spectrum for the zenith blue sky (SZ) observed by Taylor and Kerr[9] is shown along with the three spectra G, C, and S discussed above. A progressive hierarchy in spectral contours is shown extending from the global spectrum G, slightly off-white toward the yellow, to the zenith sky SZ toward the blue.

For the EC window transmittance spectra shown in B, the spectral contours are complex, with interference fringes due to the electrochromic multilayers. Trends appear both in the peak wavelength itself and on the long wavelength side of the peaks. In addition, there appears a peak shift reversal from color state 4 (460nm) to state 5 (490nm) shown by the arrows. In any case, the polychromatic complexity of both the incident sky spectra and the transmitted EC spectra requires a detailed chromaticity analysis for a proper specification of color shift.

5.1 Chromaticity analysis

A chromaticity analysis using the CIE (1931) 2° tristimulus tables[10,11] from 380nm to 780nm at 10nm wavelength intervals was made for a range of both the daylight solar spectra and the resultant transmitted spectra from the electrochromatic (EC) window with color state.

Fig. 7 shows the results of the chromaticity analysis, where A shows the total chromaticity diagram with lines of constant hue and saturation, as derived by the Stiles line element technique[10] where the constant-hue radial lines originate at the CIE source *C* point.[10] The central region relevant to the present study is expanded in the figure as shown in B. This chromaticity diagram and the chromaticity coordinates in Table 5 demonstrate the color trends of both sky and EC window. In the diagram, the relative coordinate positions are shown for four types of illuminants,

A. Daylight locus with individual incident solar spectra
B. Blackbody locus
C. CIE artificial source *C*
D. EC transmitted chromatic trajectories with color state

5.2 Daylight chromaticity

The all-sky daylight locus of chromaticity points is shown in Fig. 7B by a line that extends over a wide range and runs approximately parallel to the blackbody locus curve, as shifted slightly toward the green. This daylight locus was derived by Judd et al[12] from 622 daylight spectra under all-sky conditions, where their chromaticity points were found to cluster about a curve defined by the equation,

$$Y = 2.870\ X - 3.000\ X^2 - 0.275 \qquad (3)$$

Specific solar/sky type spectra have been observed by Taylor and Kerr[9] that include for clear sky,

A. Direct beam (DB)
B. Global horizontal (GH)
C. North sky (45° from zenith) (SN)
D. Zenith blue sky (SZ)

along with,

E. Overcast cloud (CO)

These points as well as the G, C, and S spectra points described above are plotted in the chromaticity diagram superimposed along the daylight locus curve.

A distinct spectral hierarchy for these daylight spectra is observed in Fig. 7 starting from the direct beam spectrum (DB) and proceeding toward the blue to the zenith spectrum (SZ) as,

$$DB \longrightarrow G,GH \longrightarrow C,CO \longrightarrow S \longrightarrow SN \longrightarrow SZ.$$

In addition, the individual solar/sky types show clear differences within a specific type. For example, the cloud chromaticity points, C and CO, cluster closely together in the "white" region. The sky spectra chromaticity points, on the other hand, extend over a wide range depending on the degree of sky turbidity and on the observed sector of the sky dome. For example, the model sky spectra S represents a turbid sky, with turbidity $\tau = 0.25$ and with a high water vapor content ($w = 4.80$ cm) resulting in a sky with a "whitish" hue. The "clear" sky, however, observed with direction by Taylor and Kerr shows a marked chromatic shift extending from the north sky (SN) ($x = 0.278$, $y = 0.294$) to the deeper blue zenith sky (SZ) ($x = 0.2635$, $y = 0.2785$). Overall, with the daylight chromaticity points extending over the wide range shown in Fig. 7B, these daylight chromaticity results demonstrate that any one source, such as the CIE illuminant *C* often used to simulate daylight, is highly inadequate.

5.3 EC chromaticity trajectories with color state

The transmitted spectral chromaticities were calculated for the EC window over the five color states described above. Also, incident solar spectra that are considered to be useful in window performance analyses are shown here, that include spectra G, C, S, and SZ. These spectra are incorporated to show the maximum realistic range along the daylight locus curve, as shown in Fig. 7B.

The individual chromatic trajectories progressing with increasing color state

(1 → 5), each starting from its respective incident solar spectrum point, are also shown in Fig. 7B. Each trajectory shifts toward the blue in a systematic manner up to state 4, where a sharp deviation (or "hook") appears. The overall range of chromaticity coordinates extends widely from state (1) with the G spectra (x = .3264, y = .3396) to state (5) with the SZ spectra (x = .2297, y = .2731) as given in Table 5.

5.4 Correlated color temperature with color state

The net optical behavior of the electrochromic window with color state under a range of solar/sky conditions is best understood chromatically from a study of the correlated color temperature (CCT) versus a relevant experimental parameter, such as the applied potential.

The correlated color temperature (CCT) (K), as distinguished from the color temperature, is used for chromaticity points off the blackbody locus shown in Fig. 7, but still in the vicinity of this locus. CCT values have been computed for all points in Fig. 7 from lines of constant CCT computed by K. L. Kelly.[13] The tabulated CCT results are documented for the daylight and CIE source *C* in Table 6. Correspondingly, the CCT results for the EC trajectories from transmitted spectra, with color state and with the G, C, S, SZ incident spectra are given in Table 5.

A strong dependence of the CCT upon the incident spectrum and on the applied potential was found as shown in Fig. 8. For the incident spectra, CCT in the bleached state (1) ranges from 5660K for G to 13,250K for SZ. These CCT's represent the color change that an EC window in the bleached state might experience under realistic solar/sky conditions.

The net color change (CCT) with increasing potential difference (PD), as shown in Fig. 8A, appears to undergo three distinct behavior regions:

A. Initial spectrally quiescent region from the bleached state (+1.2V on the applied potential scale) to the zero applied potential line shown in the figure, where the color change is minimal.

B. Intermediate region (states 2 → 4), where the color changes rapidly, as given for regions A to B by the power function,

$$CCT(PD) = CCT(1) + A\,(PD)^{n_1}\,, \qquad (4)$$

where the least-squares fitted curves shown in the figure have powers of n_1 = 10-12, as given in Table 7.

C. Final saturation (or breakdown) region (states 4 → 5), where there is a distinct change, believed due to an internal ion distribution shift within the EC multilayer, as yet unexplained.

The net optical behavior of the EC window is further compared with the CCT color behavior by studying the comparative visible transmittance T_V over the same potential difference (PD) scale as shown in Fig. 8B. Here again the sky-averaged T_V behavior can be divided into the same three regions discussed for CCT above, with an overall decrease from 62.7% at the bleached state (1) to a low of 25.9% at the highly colored state (5). These data also have been fitted for regions A to B by a new power function,

$$T_V\,(PD) = T_V\,(1) - B\,(PD)^{n_2}\,, \qquad (5)$$

where $n_2 = 8.0$, as given in Table 7. This general three-region correlation between Figs. 8A and 8B indicates that the spectral contour shifts with wavelength as seen in the original irradiance spectra of Fig. 6 are real and not subject to potential errors in the computational steps made to find the resultant CCT values.

6. ACKNOWLEDGEMENTS

The authors wish to thank Cheryl Kennedy for performing the spectral measurements and to Paul Wencko for programming assistance. One of us (D.E.S.) would like to thank the National Renewable Energy Laboratory for its hospitality and the Director's Development Fund for a support grant.

7. REFERENCES

1. D. E. Soule and S. W. Hodges, "Spectral solar model for instantaneous all-sky conditions based on broadband irradiation," Proc. 21st American Solar Energy Soc. Conf., Cocoa Beach, FL, pp. 299-304, June 1992.

2. Ji-Guang Zhang, David K. Benson, C. Edwin Tracy, Satyen K. Deb, A. W. Czanderna, and R. S. Crandall, "Optimization study of solid-state electrochromic devices based on WO_3/lithium-polymer electrolyte/V_2O_5 structures," Jour. Electrochem. Soc., Vol. 141(10), pp. 2795-2800, 1994.

3. C. J. Riordan, D. R. Myers, and R. L. Hulstrom, "Spectral solar radiation data base documentation," S.E.R.I./TR-215-3513 A/B, Vols. I and II, January 1990.

4. Richard E. Bird and Carol Riordan, "Simple solar spectral model for direct and diffuse irradiance on horizontal and tilted planes at the earth's surface for cloudless atmospheres," Jour. of Climate and Appl. Meteorl., Vol. 25, pp. 87-97, 1986.

5. D. E. Soule, "Daily advanced window performance from a spectral model," Proc. 14th National Passive Solar Conf., Denver, CO, pp. 316-321, June 1989.

6. ASHRAE, "Fenestrations," *ASHRAE Handbook:* 1985a Fundamentals, Atlanta, GA: American Soc. of Heating, Refrigeration and Air-Conditioning Engineers.

7. D. K. Benson, L. K. Smith, C. E. Tracy, T. Potter, C. Christensen, and D. E. Soule, "Vacuum window glazings for energy-efficient buildings: Summary report," S.E.R.I./TP-212-3684, May 1990.

8. M. Rubin, "Calculating heat transfer through windows," Energy Research, Vol. 6, pp. 341-349, 1982.

9. A. H. Taylor and G. P. Kerr, "The distribution of energy in the visible spectrum of daylight," Jour. Opt. Soc. America, Vol. 31, pp. 3-8, 1941.

10. Gunter Wyszecki and W. S. Stiles, *Color Science, Concepts and Methods, Quantitative Data and Formulas,* John Wiley & Sons, New York 1967.

11. *1993 Annual Book of ASTM Standards,* 06.01, E308-390, 1993.

12. D. B. Judd, D. L. MacAdam, and G. Wyszecki, "Spectral distribution of typical daylight as a function of correlated color temperature," Jour. Opt. Soc. America, Vol. 54, pp. 1031-1040, 1964.

13. See reference 10, pp. 55-63.

Table 1 - Electrochromic window series with color states

Color State	EC Window	Applied Potential (v)	Potential Difference (v)
1 (Bleached)	Z4D1	+1.20	0
2	Z4D2	-0.48	1.68
3	Z4D3	-0.59	1.79
4	Z4D4	-0.72	1.92
5 (Highly colored)	Z4D5	-1.80	3.00

Table 2 - Spectrally selective window series

Window	Crossection
SLS	SLS (3mm) (Standard DSA, 0.125 in. thickness)
SLSD	SLS (3mm) / Air (1mm) / SLS (3mm)
SNOD	SnO_2 coated SLS (3mm)* / Air (1mm) / SLS (3mm)
ITOD	ITO coated SLS (3mm)+ / Air (1mm) / SLS (3mm)

*Ford glass (55Ω/□), +Applied Solar glass (6Ω/□)

Table 3 - Incident irradiance spectral sky fractions

Sky	UV	NIR
G	6.6%	47.8%
C	10.5	38.1
S	13.8	28.8

Table 4 - Spectral selectivity ratios for double-glazed windows

Window	T(560nm)	T(2500nm)	T-ratio
SLSD	0.806	0.662	1.22
SNOD	0.747	0.172	4.35
Z4D1	0.637	0.0427	14.9
ITOD	0.679	0.0021	323.0

Table 5 - Chromatic trajectories with EC color state

Daylight	Color state	X-coor.	Y-coor.	CCT(K)
A. Clear global (G)	-	.3288	.3410	5.660×10^3
	1	.3264	.3396	5.770
	2	.3166	.3349	6.270
	3	.3080	.3307	6.750
	4	.2941	.3253	7.630
	5	.2819	.3371	8.180
B. Cloud (C)	-	.3180	.3281	6.210
	1	.3157	.3266	6.350
	2	.3061	.3216	6.950
	3	.2977	.3172	7.540
	4	.2843	.3114	8.660
	5	.2729	.3233	9.210
C. Turbid sky (S)	-	.2962	.3114	7.770
	1	.2942	.3098	7.940
	2	.2852	.3044	8.810
	3	.2775	.2997	9.710
	4	.2653	.2936	11.490
	5	.2553	.3058	11.740
D. Clear zenith sky (SZ)	-	.2635	.2785	13.250
	1	.2619	.2770	13.610
	2	.2542	.2714	16.450
	3	.2477	.2665	20.000
	4	.2376	.2603	28.820
	5	.2297	.2731	25.000

Table 6 - Daylight correlated color temperatures (CCT)

Direct beam spectrum	CCT(K)
DB*	5,360
Global horizontal spectra	
G	5,660
GH*	5,990
Cloud spectra	
C	6,210
CO*	6,490
Cloud+	6,480
Sky spectra	
S (turbid sky)	7,770
SN* (north clear sky)	9,970
SZ* (zenith clear sky)	13,250
CIE source spectrum	
C#	6,740

*Taylor and Kerr[9]
+Judd et al[12]
#Wyszecki & Stiles[10]

Table 7 - Parametric fit for CCT and T_V to EC window applied potential

A. CCT+	Sky	CCT(1) (K)	A	n_1	RMS error (%)
	G	5.786×10^3	0.002736	10	±2.23
	C	6.356	0.003404	10	2.35
	S	7.917	0.005247	10	1.89
	SZ	13.481	0.006091	12	1.74
B. T_V*		$T_V(1)$ (%)	B	n_2	RMS error (%)
		62.783	0.1145	8	±0.13

+See Eq. 4
*See Eq. 5

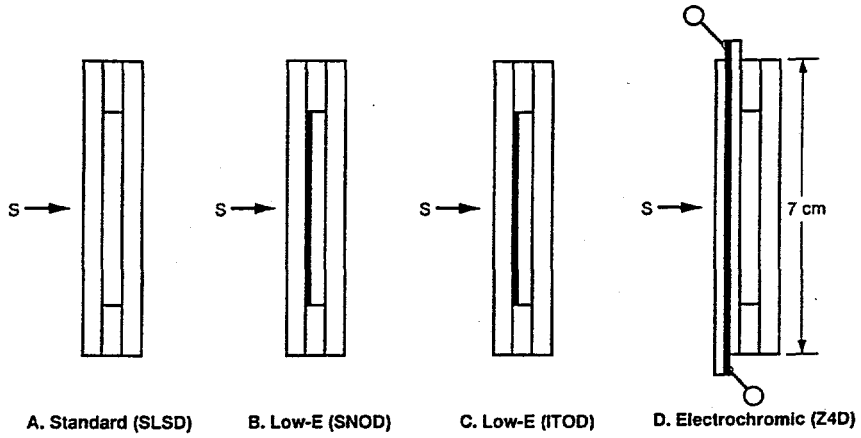

Figure 1 - Double-glazed window sections for transmittance and reflectance optical measurements. The section sequence is, A standard sodalime silicate window (SLSD), B low-E window with SnO_2-coating (SNOD), C low-E window with ITO-coating (ITOD), and electrochromic window (Z4D). The incident solar flux (S) direction is shown, where the low-E coatings (black) are located on lite surface #2 for optimal summer performance.

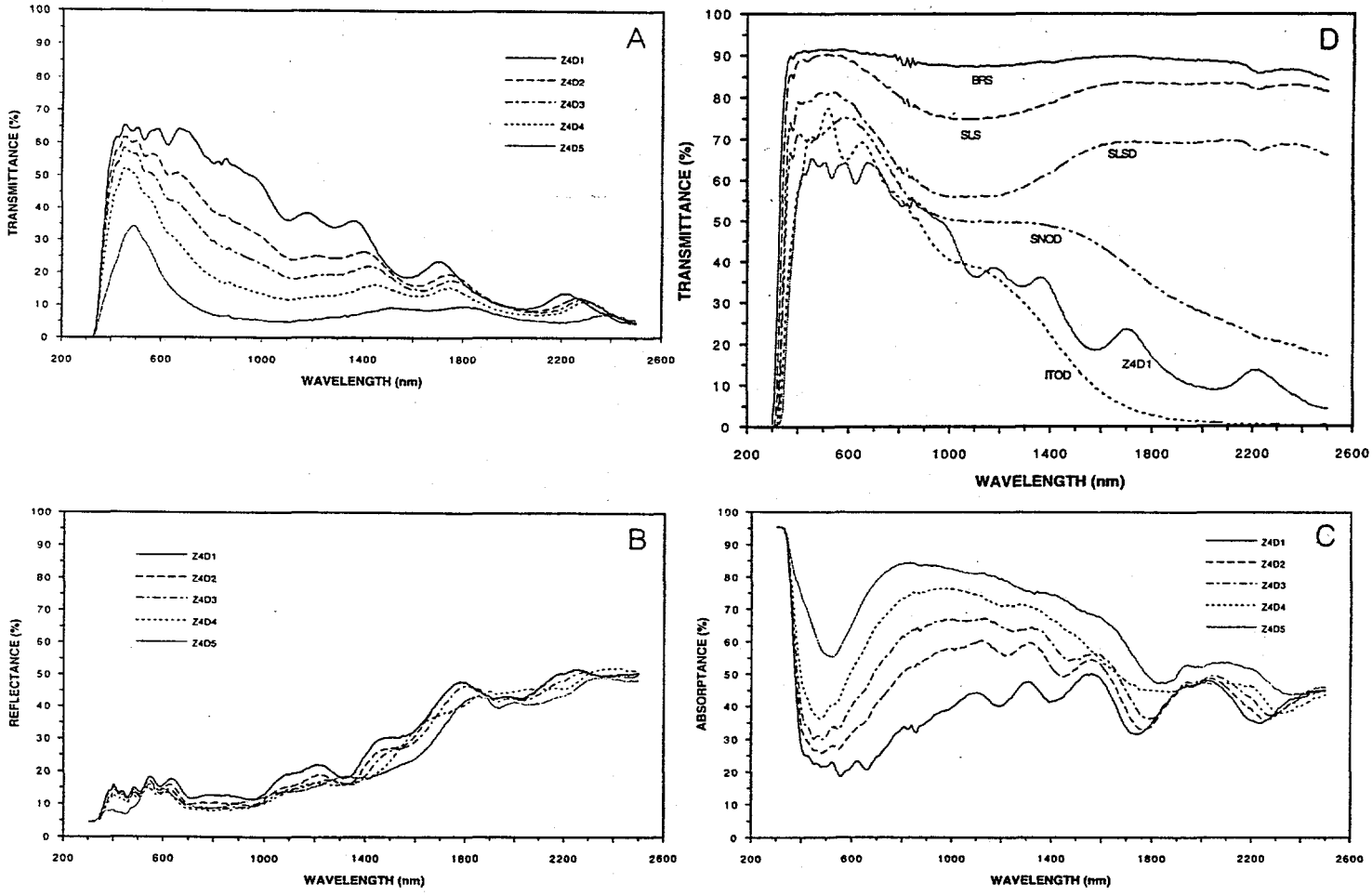

Figure 2 - Spectral $T(\lambda)$ and $R(\lambda)$ measured curves for the electrochromic window (EC) series with color state and spectrally selective (SS) series with selectivity. For the EC series, A is for $T(\lambda)$ and B for $R(\lambda)$. For the SS series, D is for $T(\lambda)$, where single-glazed borosilicate (BPS) and sodalime silicate (SLS) panes are included for reference. In C the calculated $A(\lambda) = 1 - T(\lambda) - R(\lambda)$ is given for the EC series.

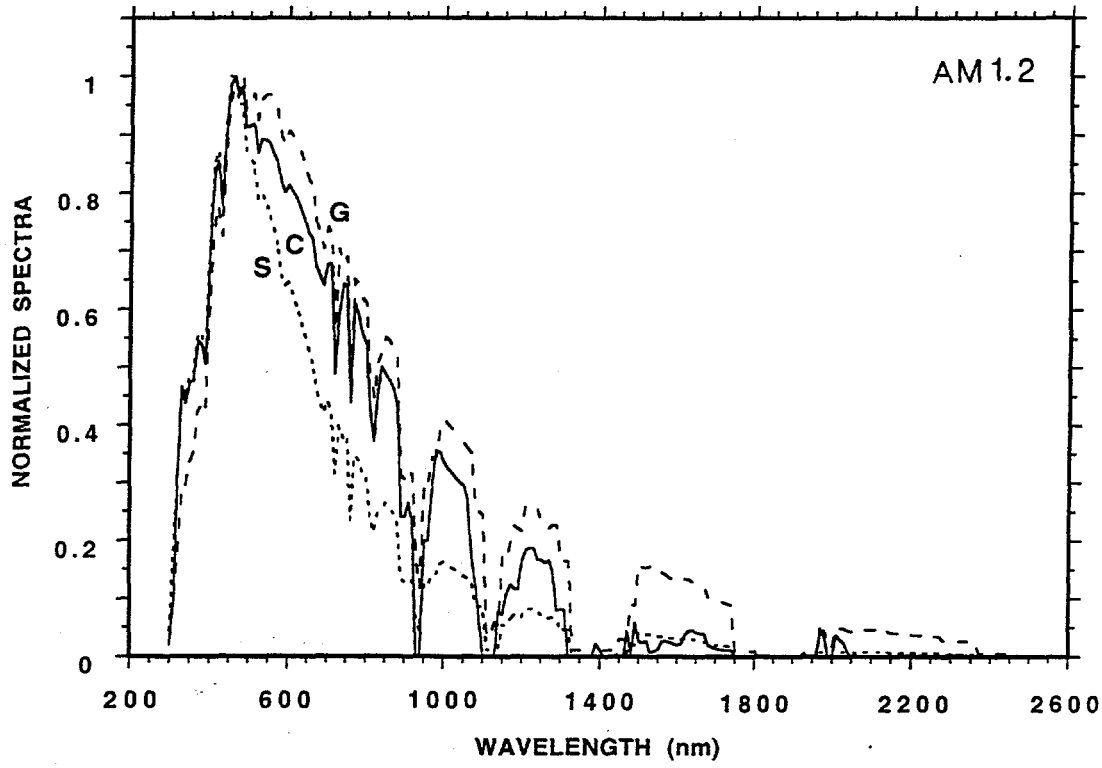

Figure 4 - Normalized all-sky model solar spectra for clear global (G), cloudy (C), and turbid sky (S), with AM1.2 solar orientation and matched atmospheric parameters.

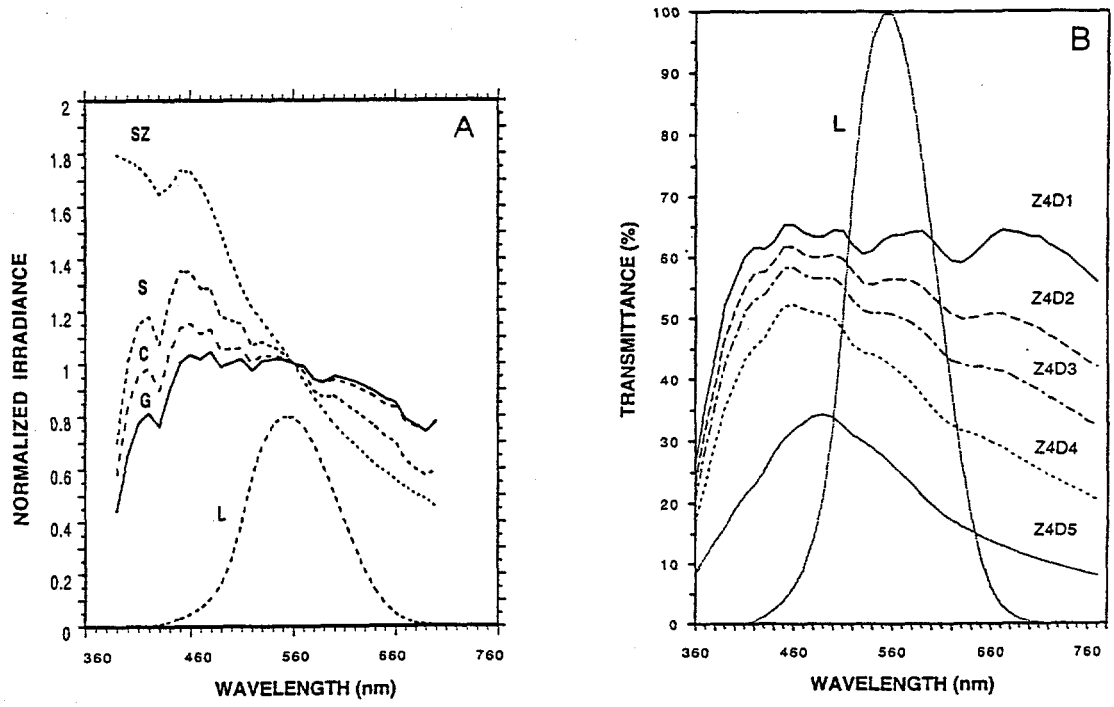

Figure 6 - Incident visible solar spectra are shown in A for clear global (G), cloudy (C), turbid sky (S) and clear zenith sky (SZ), with progressive spectral shift toward the blue. The luminous response curve (L) is included for chromatic perspective. In B the corresponding visible T(λ) of the EC window series also shows a shift toward the blue with color state (1 → 5).

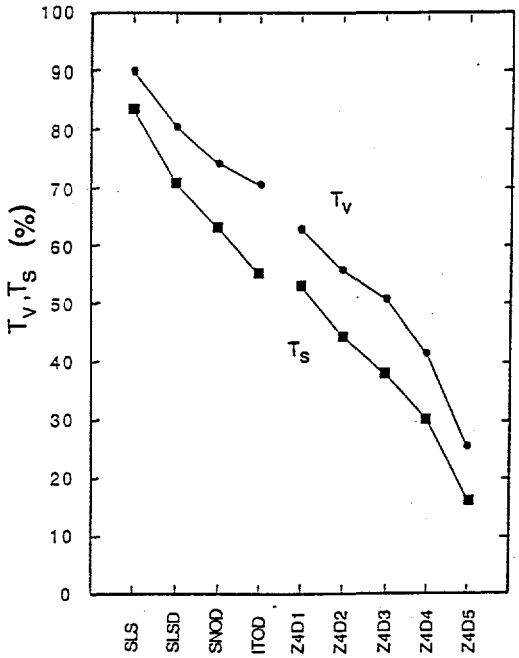

Figure 3 - Sky-averaged visible (T_V) and solar (T_S) transmittances. The SS window series is shown between SLSD and ITOD and the EC series between Z4D1 (bleached) to Z4D5 (colored).

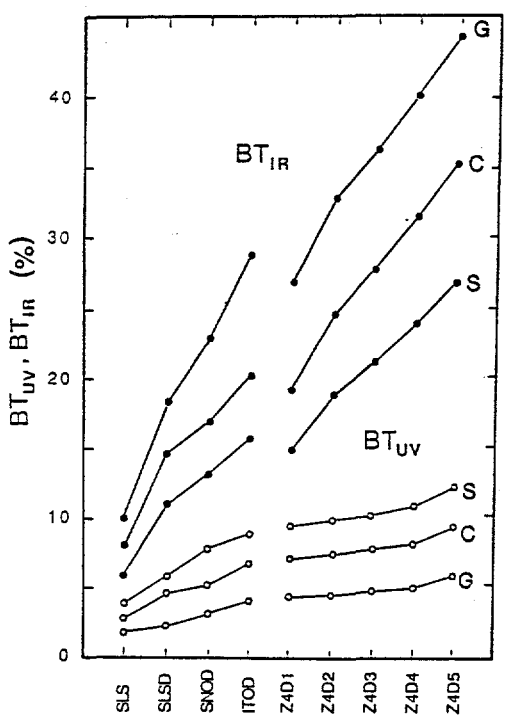

Figure 5 - Near infrared (NIR) and ultraviolet (UV) blocking fractions for incident G, C, and S solar irradiation. The SS window series is shown between SLSD and ITOD and the EC series between Z4D1 (bleached) to Z4D5 (colored).

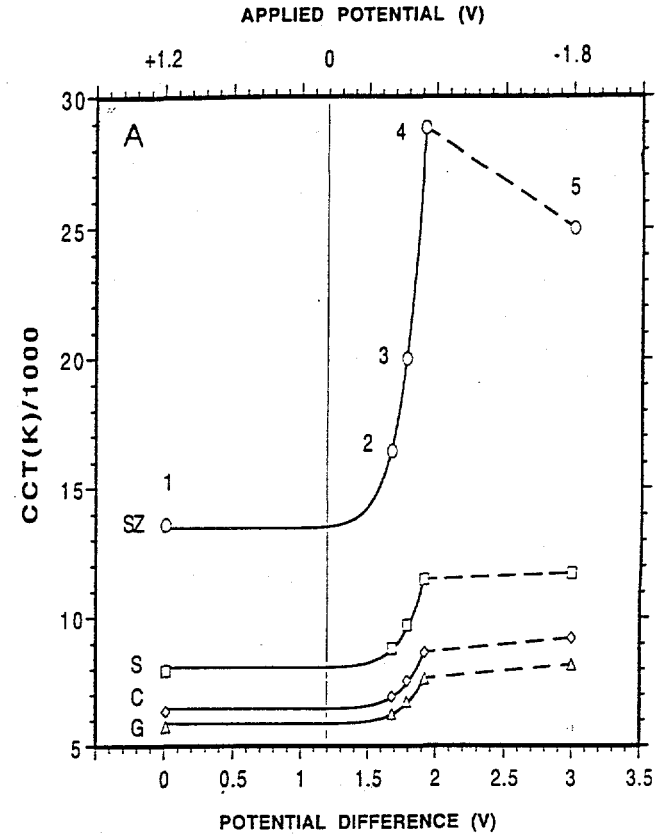

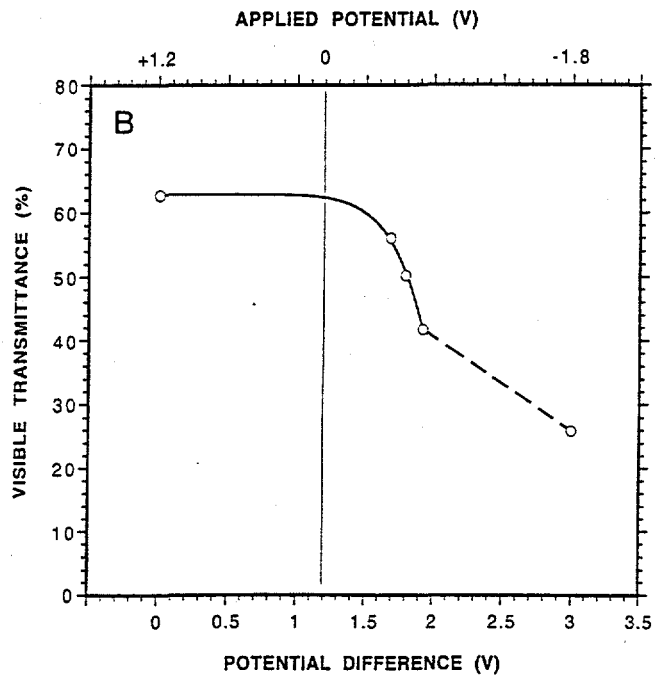

Figure 8 - Correlated color temperatures (CCT) with EC applied potential (P) in A for G, C, S, and SZ incident solar spectra and in B for the sky-averaged visible transmittance (T_V) with P for color states (1 → 5). Fitted curves from the bleached state (1) to state (4) are defined in the text for CCT by Eq. 4 and for T_V by Eq. 5.

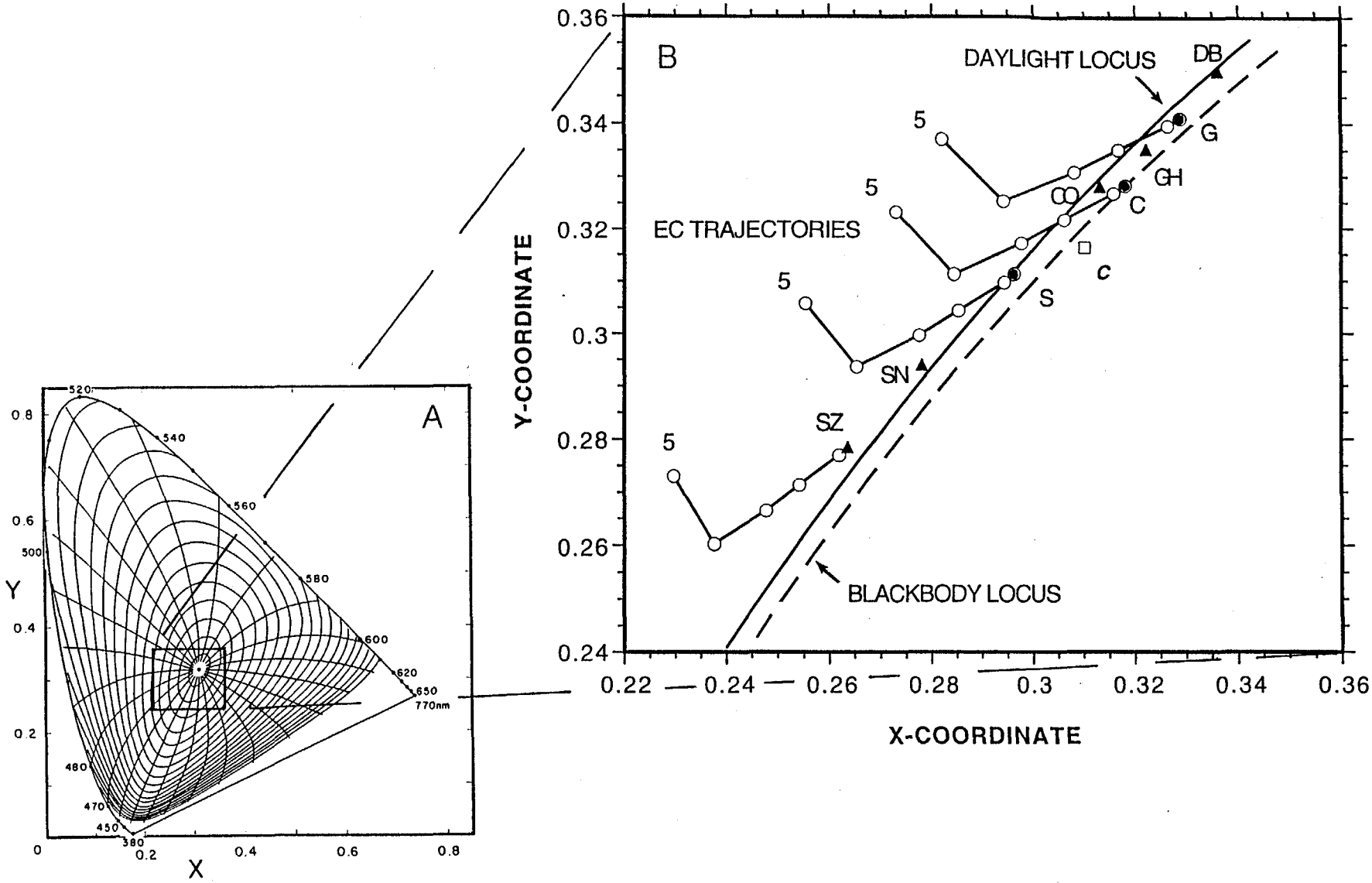

Figure 7 - Chromaticity diagram from CIE (1931) 2° analysis for incident solar spectra and resulting transmitted EC spectra with color state. In A the total chromaticity diagram is shown with radial constant-hue lines and concentric constant-saturation lines.[10] An enlarged central section is shown in B, including the blackbody locus, daylight locus,[12] daylight types (DB, GH, CO, SN, and SZ),[9] G, C, and S solar models, and EC chromatic trajectories with color state (1 → 5).